Biomaterials 48 (2015) 56–65

Contents lists available at ScienceDirect

Biomaterials

journal homepage: www.elsevier.com/locate/biomaterials

Layer-by-layer assembled cell instructive nanocoatings containing platelet lysate

Sara M. Oliveira [a, b], Vítor E. Santo [a, b], Manuela E. Gomes [a, b], Rui L. Reis [a, b], João F. Mano [a, b, *]

[a] 3B's Research Group – Biomaterials, Biodegradables and Biomimetics, Dept. of Polymer Engineering, University of Minho, AvePark, Caldas das Taipas, Guimarães 4806-909, Portugal
[b] ICVS/3B's – PT Government Associate Laboratory, Braga/Guimarães 4806-909, Portugal

ARTICLE INFO

Article history:
Received 15 September 2014
Accepted 20 January 2015
Available online

Keywords:
Layer-by-layer assembling
Instructive surfaces
Platelet lysate
Growth factors
Cell behavior
Platelet derivative

ABSTRACT

Great efforts have been made to introduce growth factors (GFs) onto 2D/3D constructs in order to control cell behavior. Platelet lysate (PL) presents itself as a cost-effective source of multiple GFs and other proteins. The instruction given by a construct-PL combination will depend on how its instructive cues are presented to the cells. The content, stability and conformation of the GFs affect their instruction. Strategies for a controlled incorporation of PL are needed. Herein, PL was incorporated into nanocoatings by layer-by-layer assembling with polysaccharides presenting different sulfation degrees (SD) and charges. Heparin and several marine polysaccharides were tested to evaluate their PL and GF incorporation capability. The consequent effects of those multilayers on human adipose derived stem cells (hASCs) were assessed in short-term cultures. Both nature of the polysaccharide and SD were important properties that influenced the adsorption of PL, vascular endothelial growth factor (VEGF), fibroblast growth factor b (FGFb) and platelet derived growth factor (PDGF). The sulfated polysaccharides-PL multilayers showed to be efficient in the promotion of morphological changes, serum-free adhesion and proliferation of high passage hASCs (P > 5). These biomimetic multilayers promise to be versatile platforms to fabricate instructive devices allowing a tunable incorporation of PL.

1. Introduction

The design of cell instructive surfaces is of major interest in the field of tissue engineering and regenerative medicine. Cell behavior is dictated by the interactions occurring between cell surface macromolecules, e.g. transmembrane proteins, glycolipids, glycoproteins and carbohydrates with the extracellular environment [1–4]. Cells are embedded in extracellular matrix (ECM), which is rich in glycosaminoglycans, proteoglycans, water and growth factors (GFs), and confers mechanical support and anchorage points. GFs are cytokines present either in soluble form or non-covalently bound to ECM polysaccharides presenting various sulfation degrees. GFs bind to cell tyrosine kinase receptors triggering intracellular events, making them very attractive molecules for cell behavior manipulation [5]. Cell behavior is affected by the concentration of GFs, as well as, by the presence or absence of their conjugations with sulfated polysaccharides [6]. GFs have a short half-life and so, strategies for their stabilization and exposure to cells at adequate doses, to trigger the adequate cell responses, are very important for many therapeutic applications [7,8]. Several methodologies for the introduction of one or two different recombinant GFs (rGFs) have been used: covalent binding [9,10], absorption [10], biotinylated heparin-avidin bonding [11], layer-by-layer (LbL) assembling [12], GF absorption onto pre-built LbL multilayers [13,14], and electrostatic binding with heparin [15,16]. However, more translational developments in this area have been hindered by the high cost of rGFs, and difficulties to introduce simultaneously several GFs.

Platelets arise as a cost-effective autologous source of multiple GFs and other bioactive proteins – Scheme 1a. Among them, some have a proven ability to improve, for instance, adhesion, mitogenesis and cell differentiation [17–19]. The instructive potential of

* Corresponding author. University of Minho, 3B's Research Group, Dept. of Polymer Engineering, Avepark – Parque de Ciência e Tecnologia, Zona Industrial da Gandra, 4805-017 Barco – Guimarães, Portugal. Tel.: +351 253510900; fax: +351 253510909.
E-mail address: jmano@dep.uminho.pt (J.F. Mano).

http://dx.doi.org/10.1016/j.biomaterials.2015.01.020
0142-9612/

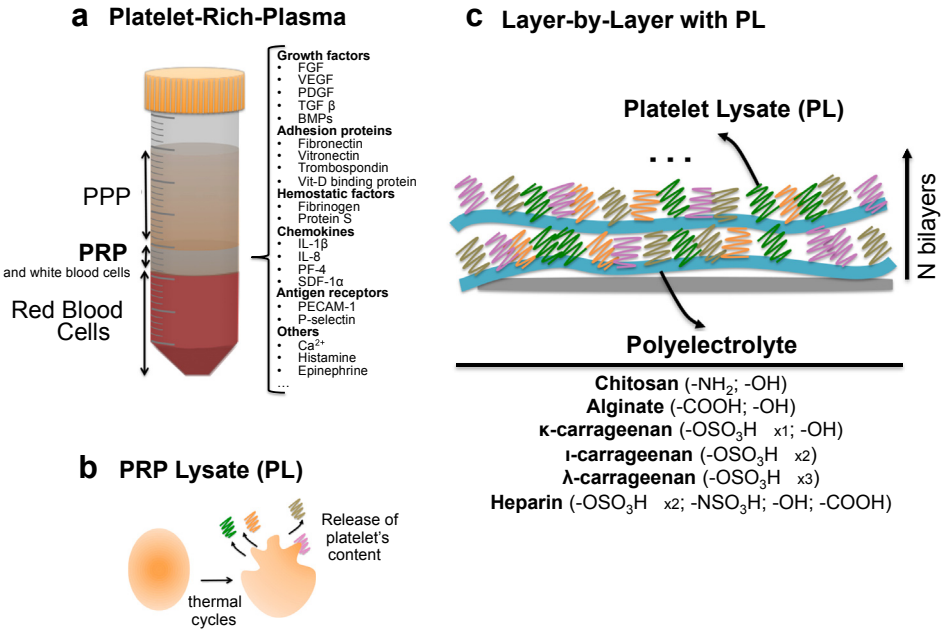

Scheme 1. Main steps for the preparation of PL/Polysaccharides Layer-by-Layer assembled nanocoatings. a) Platelet isolation from human blood as Platelet-Rich-Plasma (PRP) and examples of bioactive proteins than can be found in the enriched protein cocktail. b) PL preparation: PRP activation by platelet disruption induced by thermal cycles for the release of the inner content. c) Layer-by-Layer deposition combining PL with several PEs which respective functional groups and content are indicated.

platelet derivatives as a media supplement has been shown to vary with the GF content and also displays variability associated with the donor [20–22]. Platelet's derived GFs have been successfully included onto surfaces employing adsorption [23,24] and antigen specific GF recruitment from platelet lysate (PL) [25]. Sole absorption of GFs only allows for a short-term control over cells since, typically, they are quickly released. Covalent binding of a GF allows a more stable presentation to the cells. However, its activity may be compromised by changes in the GFs conformation, masking the active sites, or by GF-receptor complexes cell internalization inhibition [26].

LbL is a simple and versatile technology that has been employed in the development of a large variety of biomedical devices [27,28]. It is often based on a simple alternated deposition of negatively and positively charged polyelectrolytes (PEs). LbL can be performed in protein-mild conditions on virtually any substrate, ranging from nanoparticles to 3D scaffolds and hydrogels [27,28]. There are reports on the beneficial use of one or two rGFs in LbL approaches [12,29,30].

We believe that it would be advantageous to include multiple GFs from human sources as structural components of the multilayers, increasing both the complexity of the structures and the similarity with the ECM. We propose the use of LbL assembling for the development of multilayers nanocoatings containing PL in their structural composition, in which cell instructive cues can be preserved. PL was combined with several polyelectrolytes (PEs) presenting different SD (from 0 to 3 sulfate groups per sugar unit), different charges, functional groups conformation, and compared to the gold standard for protein stabilization – heparin. Heparin is a highly sulfated polysaccharide that has been widely used to stabilize and attract rGFs [15,16,31,32] and has been inspiring the synthesis of new polymeric matrices with heparin-analog ending groups [33]. PEs were assessed for their capability to adsorb PL, including the following specific GFs: VEGF, PDGF and FGFb. The role of the PE used and the bioactivity of those multilayers were evaluated by assessing its mitogenic, morphological and phenotypic effects on human adipose derived stem cells (hASCs).

2. Materials and methods

2.1. Materials

Medium molecular weight chitosan (Chi), with a degree of deacetylation of 80% (Sigma Aldrich, MKBB0566), was purified by a re-precipitation method. Briefly, Chi powder was first dissolved in 2% (v/v) acetic acid solution at a 1% (w/v) concentration. The mixture was maintained under stirring overnight at room temperature. The impurities were removed by four filtration cycles. Then, Chi was precipitated by addition of 1 M NaOH while stirring. Final steps consisted of washing Chi with distilled water until reaching a neutral pH and of dehydration by washing with ethanol–water mixtures with increasing ethanol content (20–100% v/v). Chi was freeze-dried for 3 days and grinded. κ- (Sigma–Aldrich, 22048), ι- (Fluka, 22045), λ-carrageenan (Car; Sigma–Aldrich, 22049), sodium heparin (Hep; Sigma–Aldrich, H3149), sodium alginate (Alg; Sigma Aldrich, 250 cP), and poly(ethyleneimine) solution (PEI; Sigma–Aldrich, P3143) were used as received.

2.2. Materials preparation

2.2.1. Preparation of platelet lysate

Platelet concentrates were obtained from different platelet collections performed at Instituto Português do Sangue (IPS, Porto, Portugal), under a previously established cooperation protocol. The components were obtained using either the Trima Accel® Automated Blood Collection System. All the platelet products were biologically qualified according to the Portuguese legislation. The platelet count was performed at the IPS using the COULTER® LH 750 Hematology Analyzer and the sample volume adjusted to 1 million platelet.μL^{-1}. The collected samples were subject to three repeated temperature cycles (frozen with liquid nitrogen at −196 °C and heated at 37 °C) and frozen at −20 °C until further use. The remaining platelets were eliminated by centrifugation at 1400 *g* for 10 min. Aliquots of platelet lysate (PL) were stored at −20 °C until final use.

2.2.2. Polyelectrolytes solutions

κ-,ι-, λ-Car, Hep and Alg were prepared in 1 M Tris HCL 40 nM NaCl pH 7.4 with a concentration of 0.5 mg.mL^{-1}. Chi was dissolved in sodium acetate buffer with a concentration of 0.5 mg mL^{-1}. All the solutions were gently stirred overnight. PL was 10-fold diluted with Tris HCL buffer or in 1 M sodium acetate 40 mM NaCl pH 6 when to be combined with Chi.

2.2.3. QCM-D monitoring

A Q-Sense E4 quartz crystal microbalance (QCM-D, Q-Sense AB, Sweden) with dissipation was used for *in situ* monitoring the deposition of PE/PL bilayers at the surface of 100 nm gold-coated crystals. The crystals were first cleaned in an ultrasound bath at 30 °C, and immersed successively in acetone, ethanol, and isopropanol. All crystals were initially modified with PEI to confer an initial positive charge. A 0.5% w/v PEI solution (Mw 750,000, Sigma–Aldrich) was pumped for

approximately 30 min following by extensive rinsing. The initial layer in the case of the combination Chi/PL was Alg.

The different polysaccharides were assembled with PL at pH 7.4, or 6 in the case of Chi, in the respective buffer solutions above mentioned. Briefly, AT cut quartz crystals were excited at multiple overtones (1, 3, 5, 7, 11, and 13), which correspond to 5, 15, 25, 35, 45, 55 and 65 MHz, respectively. The PEs solutions (0.5 $mg.ml^{-1}$) were pumped with a constant flow rate of 50 $\mu L\ min^{-1}$, for 10 min at room temperature. As intermediate step, the respective buffer solutions were pumped during 10 min to rinse the crystals.

2.2.4. Coatings preparation in 48-well plates

48-well plates were modified with 0.5 mL of 0.5% (w/v) PEI solution to confer a positive surface charge. Then, the solution was removed and the wells were extensively rinsed with distilled water in order to remove the unbound PEI. The LbL was started by the adsorption of the negative PE. In the case of Chi, an Alg layer was first adsorbed. The adsorption times and volumes used were: 4 min and 0.5 mL for the polysaccharides solutions; 0.5 mL and 10 min for the PL solution; intermediate rising steps ×2 for 30 s using the respective buffers. The sequence was repeated 6 times. The well plates were let to air-dry overnight and then sterilized using a UV light for 40 min.

2.2.5. Protein adsorption

6-well plates were modified with PEI and the PEs, as described before. Two milliliters of PL 10% (v/v) or PL 100% (v/v), pH 6 and pH 7.4, were added to each well and let to adsorb for 30 min. The volume was removed and stored at −20 °C for further quantification. Each well was rinsed with 2 mL of the respective buffer, which was then stored for further protein quantification.

The total protein was quantified in the following solutions: initial PL, PL before and after adsorption, and rising solutions. The measurements were performed using a NanoDrop 1000 Spectrophotometer (Thermo Scientific). The absorbance of 2 μL volume of solution was measured at the wavelength 280 nm ($n = 6$). The amount of PDGF (PL10%), FGFb (PL100%) and VEGF (PL100%) was quantified using ELISA kits following the assay protocol provided with the kit. Optical density was read at 450 nm ($n = 6$) on a multi-well microplate reader (Synergy HT, Bio-Tek Instruments).

2.3. Cell behavior assessment

2.3.1. hASCs isolation

Human subcutaneous adipose tissue samples were obtained from lipoaspiration procedures performed on women with ages between 35 and 50 years under a protocol previously established with the Department of Plastic Surgery of Hospital da Prelada in Porto, Portugal. All the samples were processed within 24 h after the lipoaspiration procedure. hASCs were enzymatically isolated from subcutaneous adipose tissue as previously described [34]. Briefly, the lipoaspirate samples were firstly washed with a solution of PBS and 10% Antibiotic/Antimycotic. Liposuction tissue was digested with 0.2% Collagenase Type II solution for 90 min with intermittent shaking, at 37 °C. The digested tissue was filtered using a 100 μm filter mesh (Sigma–Aldrich, Germany). The floating adipocytes were separated from the precipitation stromal fraction by centrifugation at 1250 rpm for 10 min. The cell pellet was re-suspended in lysis buffer for 10 min to disrupt the erythrocytes. After a centrifugation at 800 rpm for 10 min, cells were again re-suspended and placed in culture flasks with Minimum Essential α Medium (Sigma–Aldrich) supplemented with sodium bicarbonate, antibiotic/antimycotic and 10% of Fetal Bovine Serum (Life Technologies). Cells were cultured until confluence at 37 °C, 5% CO_2 incubator, changing the medium every 2 days.

2.3.2. Cell seeding

To proceed with the cell seeding, expanded cells were harvested by trypsinization and filtered with a 100 μm cell strainer to remove possible cell aggregates. Two cellular suspensions with a density of 1×10^4 $cells.mL^{-1}$ were prepared in minimum essential α medium supplemented with 0% or 10% FBS. A volume of 500 μl of cell suspension was dripped into each well. Well-plates were incubated for 20 h or 4 days for the assessment of cell adhesion, morphology, proliferation, ALP activity/cell and phenotype, without changing the medium. hASCs from two different donors and between passage 5 and 6 were used.

2.3.3. Cell morphology

After 20 h in culture, samples were gently rinsed twice with sterile PBS and then fixed with formalin 2.5% (v/v) during 20 min. Cells were permeabilized with 0.5 mL of Triton 0.2% (v/v) in PBS during 2 min and then rinsed with PBS. Samples were incubated in the dark with 100 μL of (1:100) Phalloidin-TRITC (Sigma–Aldrich) solution for 30 min and then washed with PBS. For cell nuclei staining, well plates were incubated in the dark for 5 min with 100 μL 4,6-diamino-2-phenyindole dilactate (DAPI, Sigma–Aldrich) diluted 1:1000 in PBS. Samples were observed using an inverted Axio Observer Fluorescence Inverted Microscope (Zeiss).

2.3.4. Cell morphology analysis

Cell length, width and mean area were measured using the Image J software version 1.48. Cell length was considered the longest distance between the tips of the filopodias ($200 < n < 300$ cells from 8 images). The width was measured on the cell nucleus position and usually in an angle approximately right to the cell length ($200 < n < 400$ cells from 8 images). Cell area was calculated dividing the total number of nucleus by the total area covered by the same cells ($n = 8$). Cell aspect ratio was calculated by diving cell length per cell width.

2.3.5. dsDNA quantification

In order to quantify cell attachment and proliferation after 20 h and 4 days in culture, dsDNA was quantified using the Quant-iT™ PicoGreen® dsDNA assay kit (Molecular Probes/Invitrogen) that allows the measurement of the fluorescence produced when PicoGreen dye is excited by UV light while bound to dsDNA. After incubation periods, the well plates were gently rinsed once with sterile PBS. Then, 1 mL of ultra-pure sterile water added and kept at −80 °C until quantification. For the quantification, samples were defrosted at room temperature and the content was transferred to eppendorfs. 100 μL of Tris–EDTA buffer were transferred into a white opaque 96-well plate. Samples were vortexed and 28.8 μL of each plus 71.2 μL of PicoGreen solution were added to the wells. After 10 min of incubation in the dark, the plate was read in a microplate reader using an excitation wavelength of 485 nm and emission wavelength of 528 nm. A standard curve was created by varying the concentration of standard dsDNA standard from 0 to 2 $mg.mL^{-1}$, and triplicates dsDNA values of the samples were read off from the standard graph. At least six specimens were measured per each sample. The experiment was repeated once more.

Cell proliferation was calculated by assuming as 1-fold the difference between the dsDNA content at 20 h and 4 days in TCPS.

2.3.6. ALP quantification

ALP activity was quantified in the same samples used for dsDNA quantification. The activity of ALP is typically evaluated using the p-nitrophenol assay. Paranitrophenyl phosphate, which is colorless, is hydrolyzed by alkaline phosphatase enzyme at pH 9.8 and 37 °C to form free p-nitrophenol, which is yellowish. The reaction was stopped by addition of NaOH and the absorbance read at 405 nm. Briefly, in each well 20 μl of each sample, previously vortexed, were mixed with 60 μl of the substrate solution which is 0.2% (w/v) p-nitrophenyl phosphate (Sigma–Aldrich) prepared in a substrate buffer of 1 M diethanolamine (Sigma–Aldrich) at pH 9.8. The plate was then incubated in the dark for 45 min at 37 °C. After the incubation period, 80 μl stop solution, which is composed by 2 M NaOH (Panreac) plus 0.2 mM EDTA (Sigma–Aldrich), was added to each well. Standards were prepared with 10 $\mu mol\ mL^{-1}$ p-nitrophenol (pNP, Sigma, USA) solution, to obtain a standard curve covering the range 0–0.2 M. Triplicates of each sample and the standard were made. Finally, absorbance was read at 405 nm in a microplate reader (Bio-Tek, Synergie HT) and sample concentrations in triplicate were read off from the standard curve. The ALP concentrations were normalized against the dsDNA concentrations of the same samples to determine the cellular ALP activity.

2.3.7. Flow cytometry

Flow cytometry was performed using anti-human CD90 APC (BD Pharmingen™), anti-human CD105 FITC (BioRad), anti-human CD73 PE (BD Pharmingen™), anti-human CD34 PE (BD Pharmingen™), anti-human CD31 APC (R&D Systems), anti-human CD45 FTIC (BD Pharmingen™). Experiments were performed using hASCs in passages between 5 and 6, before the seeding and after 4 days in culture on the unmodified and modified surfaces.

Cells were trypsinized, counted and re-suspended in PBS with 2% (w/v) bovine serum albumin (BSA) (Sigma) with a concentration of 2×10^5 cells/100 μL and incubated with the antibodies at the concentration advised by the manufacturers. After incubation for 20 min at room temperature, protected from light, cells were washed with PBS/BSA, re-suspended in PBS with 1% formaldehyde (Sigma) and analyzed in a BD FACSCalibur™ flow cytometer (BD Biosciences). Cells of interest were gated in a forward vs. side scatter dot plot with a linear scale. Isotype controls were made to discern non-specific from specific staining. A minimum of 10,000 gated events were acquired and labeled cells were quantified.

CD's variations were calculated relatively to their initial content in the hASCs before seeding, for each sample. The calculation consisted in the difference between the percentages of each CD before and after 4 days in culture, for both donors.

2.4. Statistical analysis

First, it was verified with Shapiro–Wilk test that most of the data did not passed the normality test. All data was statistically analyzed by using non-parametric tests. The unpaired one-tailed t-test with Welch's correction for non-parametric data was used ($p \leq 0.05$).

Spearman's Correlation was computed to assess the relationship between several variable pairs to verify the existence of any positive or negative monotonic correlation, using Graphpad Prism.

3. Results and discussion

3.1. Nanocoatings assembling

LbL assembling is a versatile and simple technique in the context of cell–surface interactions design. This work has focused on the development of cell instructive multilayers prepared by combining distinct polysaccharides with proteins derived from human PL – Scheme 1a, b. Nature offers a wide range of PEs with several molecular properties that may affect the PL adsorption regarding several aspects, including: the total adsorbed PL, the amount of each GF, the net charge of the proteins, as well as, their stability. Sulfated polysaccharides are good candidates for GFs stabilization by preserving both their conformation and bioactivity through the favorable interactions with sulfate or sulfonic groups [35–37]. Herein, PEs with varying charge and number of

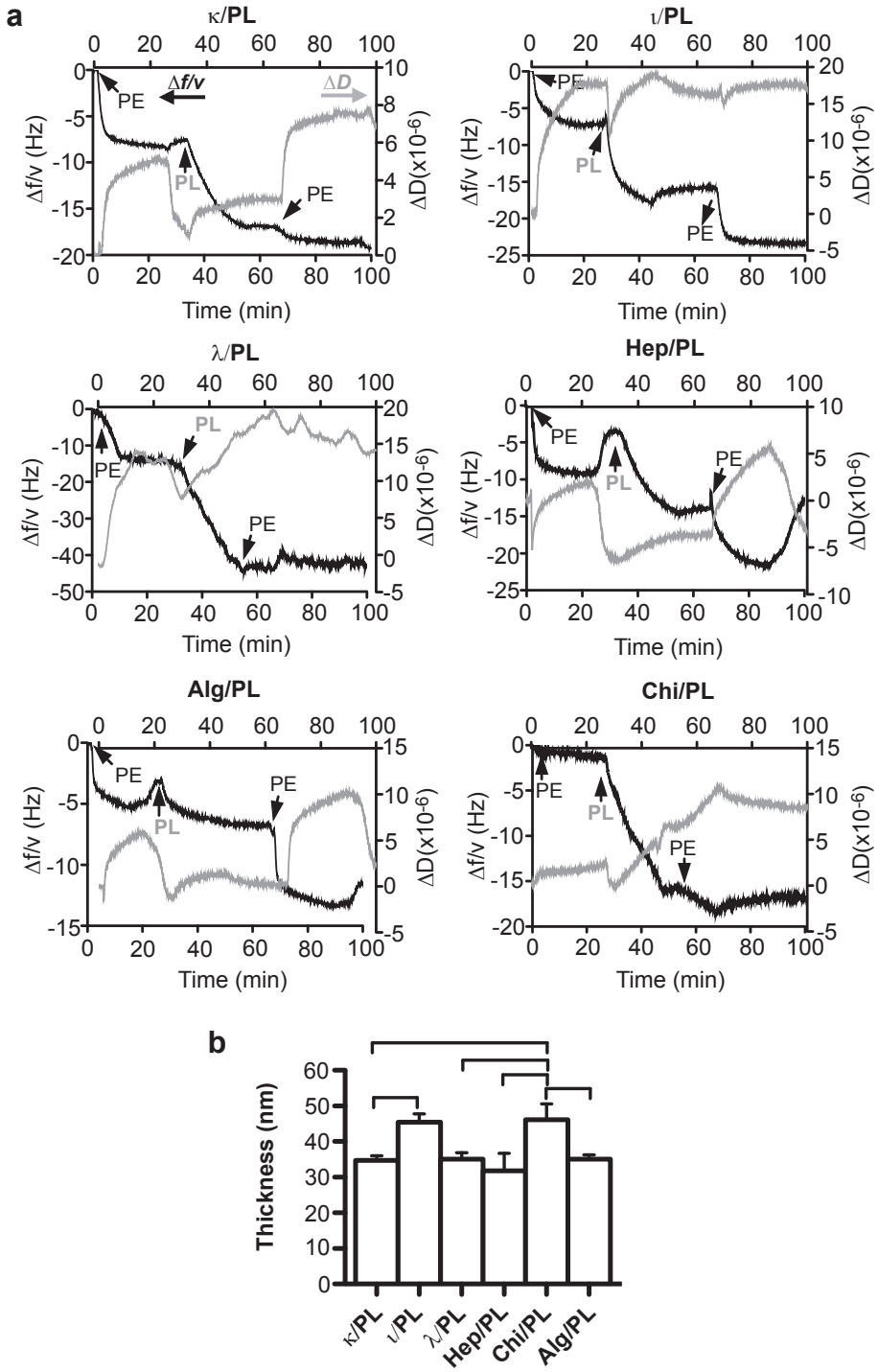

Fig. 1. Nanocoatings characterization: a) QCM-D monitoring of the normalized frequency ($\Delta f/\nu$) and dissipation (ΔD), obtained for the seventh overtone for the LbL deposition of PE-PL-PE and intermediate rinsing steps; b) Thickness of the nanocoatings with 6 bilayers measured by ellipsometry (n = 6; mean ± SEM). All combinations of pairs of samples were compared and bars indicate the statistical different ones ($p < 0.05$; n = 6; data represented as mean ± SEM).

functional groups were selected: alginate (Alg; −1) and chitosan (Chi; +1), as unsulfated ones; and κ-, ι-, and λ-carrageenan (κ, ι, λ-Car; −1, −2, −3 respectively), as sulfated ones; along with heparin (Hep; −3), as control – Scheme 1c. We hypothesize that the chemical diversity of such PEs will allow tuning of the incorporation of bioactive factors from PL and, consequently, cellular response.

The assembling of the PE/PL combinations was monitored using QCM-D – Fig. 1a. It was observed that proteins from PL (10% v/v) adsorbed independently of the PE charge or SD. Alg/PL, Chi/PL, κPL, ιPL, λPL and Hep/PL nanocoatings, with 6 bilayers, were assembled on silicon wafers. The mean thicknesses were measured by ellipsometry on dried samples – Fig. 1b. These varied between 30 and 50 nm, being similar among most of the conditions. The nanocoatings produced with the positively charged PE, Chi, were shown to be the thickest ($p < 0.05$) though similar to the one containing ι/PL. A large fraction of the PL proteins are negatively charged in a pH range of 5.5–6 (as opposed to several GFs), which may explain the higher thickness of Chi/PL nanocoatings. The multilayers were amenable to being produced using negatively charged PEs as well. Electrostatic interactions should contribute significantly to the stabilization of the multilayers, although other kinds of interactions could participate in the LbL construction, such as, hydrophobic or hydrogen bonds [38].

Total protein quantification indicated that the profile of protein adsorption may be affected by PL concentration – Fig. 2a, b. With PL 10% (v/v), Chi and κ could adsorb a higher content, as compared to all other PEs ($p < 0.05$). Increasing the PL concentration, from 10% to 100%, highly increased the content of protein ($p < 0.005$; 3–5 fold) on the unsulfated and on the more sulfated PEs (SD = 3).

The binding of specific GFs, namely PDGF, FGFb and VEGF, was investigated – see Fig. 2 c, d and e, respectively. The type of PE revealed to have a huge impact in the total content of PL, as well as, in the incorporation of the GFs. Even though sulfate groups are appropriated to bind GF through electrostatic interaction, higher SD may not imply higher adsorption. Actually, the densities of VEGF and FGFb did not correlate with the SD, nor with the total protein adsorbed – Table S2. Moreover, the adsorption of PDGF tended to decrease with the increase of the SD. Consequently the VEGF/PDGF and FGFb/PDGF ratios were increased with the increase of the SD – Table S2. Nevertheless, when comparing with the unsulfated, the sulfated ones and Hep could achieve high levels of GFs adsorption. But, interestingly, they have shown different adsorption abilities. Hep could adsorb a high content of VEGF, while κ was more prompt for a high PDGF and intermediate VEGF adsorption. On the other hand, ιCar achieved the highest levels of VEGF, FGFb and PDGF adsorption. Contrarily, λ Car has not shown the ability to highly adsorb any of the quantified GFs.

In general, the total content of protein adsorbed did not allow predicting of the respective content of GFs incorporated. In fact, several significant differences were detected in the PL layer relatively to its local density of VEGF, FGF and PDGF – see Fig. 2 f and Table S1. The PEs showed different patterns for the incorporation of GFs. This highlights the importance of the initial surface chemistry regarding the interaction of platelets derivatives with biomaterials.

Overall, the ratios of GFs can be varied with the PE, as well with the SD. This may represent a simple way of adjusting or improving the cell instructive cues of 2D/3D biomaterials, according with the target applications.

3.2. Cell morphology

Stem cell cytoskeleton organization has been correlated with cell fate commitment, besides being informative about cell senescence [39–42]. The proliferation rate of stem cells decays with increasing number of passages, and ultimately cells reach a senescent state. In the case of mesenchymal stem cells, senescence is

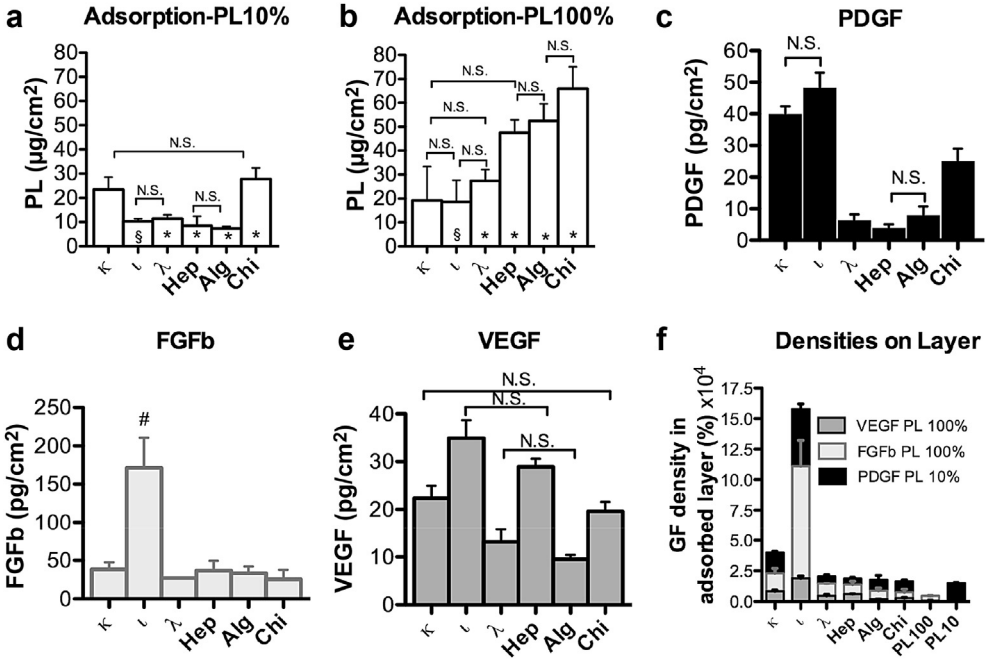

Fig. 2. Quantification of PL, VEGF, bFGF and PDGF adsorption onto different PEs layers. Total protein adsorbed accordingly with initial PL concentration: a) PL 10%(v/v), b) PL 100% (v/v). Content of GF adsorbed: c) PDGF, d) bFGF, e) VEGF. d) Density of GFs in the formed protein-layer. All combinations of pairs of samples were compared and only the pairs not statistically similar (with $p > 0.05$) are indicated with exception of d) where # represents the only significant differences ($p < 0.05$): ι is significantly different to all the other samples. In a) and b), § and * mean significant difference between the total protein adsorption with PL 10% and PL 100% with p(<0.05) or p(<0.005), respectively. Statistical analysis of f) can be consulted in Table S1. Data represented as mean ± SEM; n = 6.

defined by an enlarged morphology (larger width), reduced expression of surface markers and decreased differentiation potential [43].

The potential of the developed nanocoatings to induce any significant changes on the morphology was assessed by characterization of the width and length – Fig. S1, cell aspect ratio (length/width) and mean area –Fig. 4, after 20 h of culture – Fig. 3a. In our study, hASCs (P6-7) cultured on TCPS were approximately 50 μm wide – Fig. S1 a, b. The presence of SO_3H end groups reduced cell width in comparison with TCPS. Introducing PL on the nanocoatings further decreased the cell width for almost half of what was measured in TCPS. Correlation's analysis suggested that there was a moderate correlation between FGF/VEGF and FGF/PDGF ratios with cell width – Table S2. Among the sulfated-PL nanocoatings, cell width tended to reduce when the ratio of FGF/VEGF was increased, when FGF/PDGF was decreased and VEGF density was lowered – Table S2.

On the other hand, hASCs length tended to increase with the presence of SO_3H – Fig. S1 c, d. Comparing these with the respective surfaces with PL, its presence did not significantly alter cell length, with exception of λ/PL and Hep/PL nanocoatings where it was a slightly decreased ($p < 0.05$). The increased cohesion between cells with the incorporation of PL may have masked the tips of the filopodia and/or actually reduced cell length on those two samples. Nevertheless, Spearman's correlation pointed out that cell length tended very strongly to increase with increase of PDGF and PL, which simultaneously, represented a decrease in VEGF/PDGF and FGF/PDGF ratios.

All the width and length variations induced by the presence of the multilayers led to a huge reduction on cell mean area by 1/4 to

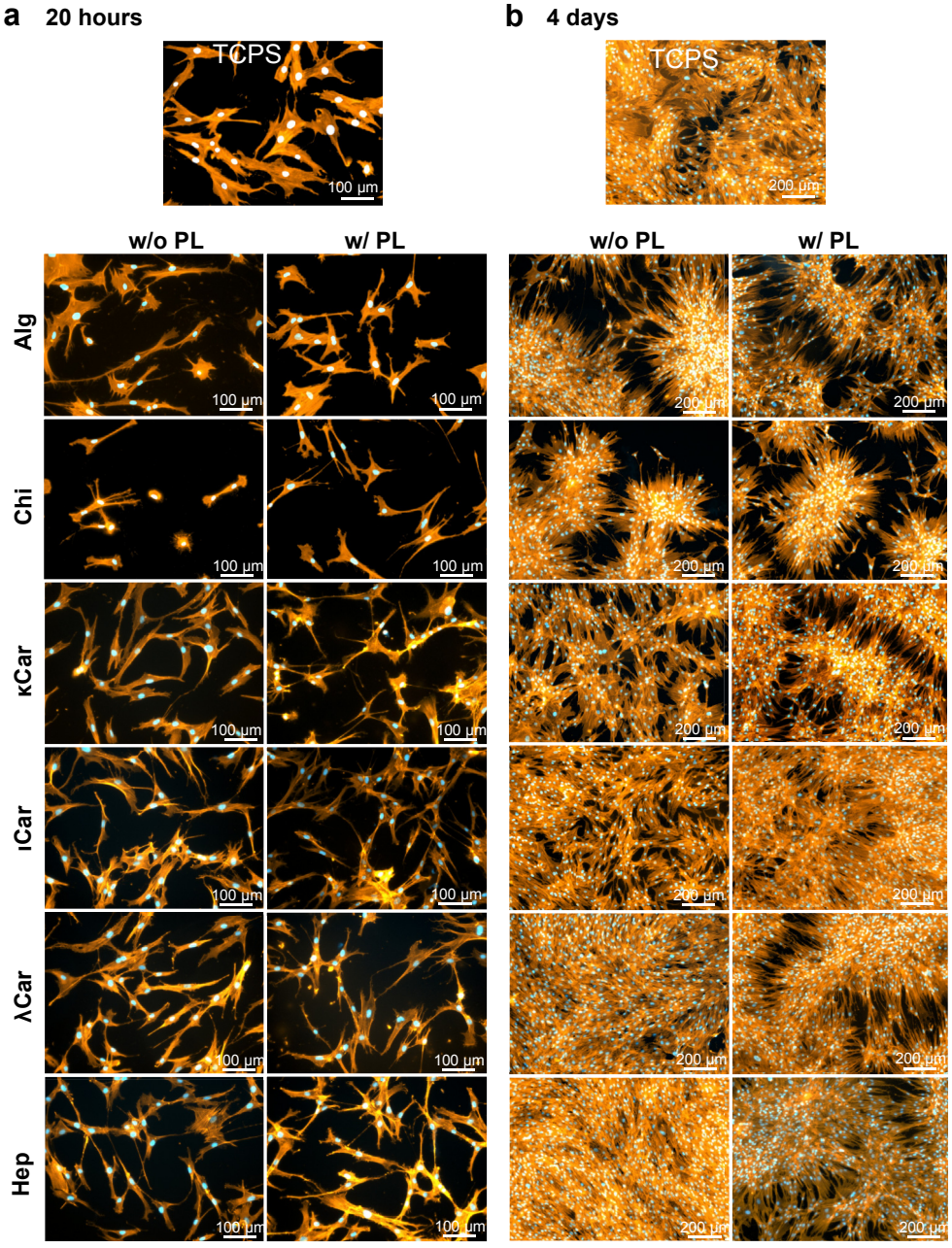

Fig. 3. a) hASCs morphology after 20 h and b) 4 days in culture, in presence of 10% of serum. (Blue – nuclei; orange – cytoskeleton). (For interpretation of the references to color in this figure legend, the reader is referred to the web version of this article.)

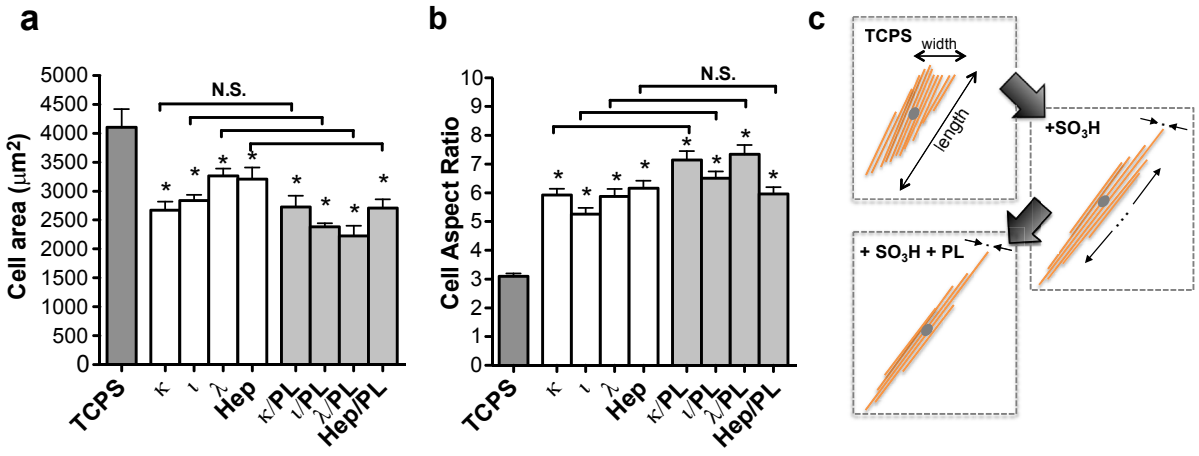

Fig. 4. hASCs morphological analysis after 20 h in culture. a) Mean cell area. b) Cell aspect ratio (Length/width). c) Scheme evidencing cell length and width behavior observed with the presence of SO_3H groups and PL. All the significances are identified: bars (the samples are different), * (samples are statistically significantly different comparing to TCPS); ($p < 0.05$; $n = 8$ cell area; $200 < n < 300$ cell aspect ratio).

1/2 from the initial 4000 μm^2 on TCPS. However, the cytoskeleton was elongated, representing an increased aspect ratio (length/width) – Fig. 4 a, b.

Overall, the presence of SO_3H on the surface made the cells achieve a slightly higher length and smaller width that further diminished when PL was incorporated. Consequently, cell aspect ratio was increased to 6–8 on the multilayers containing PL – Fig. 4 c. The developed nanocoatings reverted the enlarged morphology observed on TCPS.

3.3. Cell adhesion, proliferation and ALP activity

In order to verify the bioactive ability of the developed multilayers, their effect over hASCs adhesion and proliferation was assessed in short-term cultures – Fig. 5.

48-well culture plates were modified with PE, and PE/PL multilayers with 6 bilayers. Cells were seeded at an initial density of 5000 cells.cm^{-2} in the presence and absence of serum proteins.

In the absence of both PL and medium serum, cell adhesion was very limited and almost no differences were detected between TCPS and the PEs coatings – Fig. 5 a. The presence of PL significantly increased cell adhesion in the cases of κ/PL and ι/PL, by 5 and 8-fold, respectively, as compared to TCPS ($p < 0.05$). This suggested that those might be the nanocoatings which are richer in cell-adhesive moieties, or that cell adhesion could have been mediated by interactions between surface PDGF and cell PDGF receptors. When serum was included in the culture media, cell attachment was not as affected by the presence or absence of PL ($p > 0.05$) – Fig. 5 b. However, the surfaces containing PL, namely ι/PL and Hep/PL, allowed for a higher cell attachment than TCPS ($p < 0.05$).

The proliferation rate of hASCs usually decreases with increasing passage number. PL media supplementation has been reported to enhance cell proliferation and even refresh high passage cells [44,45]. We believe that the expansion of high passage hASCs onto the PL-multilayers might be a way to increase the proliferation ratio and avoid/delay senescence. hASCs (passage 5–6) were, therefore, cultured on the developed nanocoatings. dsDNA quantification and proliferation ratios upon 4 days of culture are shown in Fig. 5 c and Fig. 6 a, respectively. Overall, hASCs were able to proliferate on all the surfaces, and to reach over-confluence on the coatings with more SO_3H groups and PL – Fig. 3 b. Those also allowed a higher hASCs proliferation as compared with TCPS. Regarding the multilayers, ι/PL and Hep/PL have shown the highest ability to improve cells proliferation ($p < 0.05$; ~2 fold relatively to TCPS) – Fig. 6 a. Chi/PL nanocoatings were the only samples whose proliferation was impaired ($p < 0.05$). This suggests that solely Chi, or a positively charged PE, may not be adequate to attract bioactive proteins suitable to promote cell proliferation. Moreover, since Chi is uncharged during the culture, it may not ensure sufficient stabilization, or an adequate conformation of the adsorbed bioactive proteins.

The mitogenic induction can be accomplished by supplementing culture medium with GFs, such as VEGF [46], FGF [47], PDGF [48–50] and EGF [47], in a dose-dependent manner. Those mitogenic GFs can be found in PL, which is already established as medium supplement, to improve cell proliferation. Its mitogenic potential has been correlated with the concentration of PDGF [48]. As shown in the previous section, depending on the PE, the percentage of the mitogenic GFs cannot be assumed as equivalent to the total content of proteins adsorbed. Moreover, the sole ability of the PE to attract a specific GF may not be a good proliferation predictor factor if the PE itself improves cell proliferation. For example, proliferation on Hep surfaces was higher when compared with the other coatings without PL. The ability of Hep to improve cell proliferation has also been reported elsewhere [51,52]. By verifying the existence of correlations between GF surface density and cell proliferation, it was possible to detect a moderately positive correlation with VEGF and FGF. A higher ability of the PE to adsorb VEGF or FGF may be a moderate indication of a higher cell proliferation – Table S2. In addition, the morphological features showed to be correlated with proliferation. Cell proliferation tended to be higher on cells with higher cell aspect ratios and with decreased widths. In general, the culture of hASCs on these PL-multilayers has reverted the enlarged morphology, which is a senescence-associated feature, and has increased cell proliferation.

In vitro, alkaline phosphatase (ALP) is highly expressed in early osteogenesis, and is also considered a universal pluripotent marker for all types of pluripotent stem cells including embryonic stem cells, embryonic germ cells and induced pluripotent stem cells [53,54]. In hASCs, a significant increase in ALP activity during normal medium conditions suggests a cell-commitment to the osteoblastic lineage or cell aging [55]. Therefore, when solely expanding multipotent stem cells, a highly significant ALP increase might be unwelcome since it may compromise stemness. The ALP activity per lysed cell was quantified after 20 h and 4 days in culture – see Fig. 6 b. ALP significantly increased ($p < 0.05$) with increasing

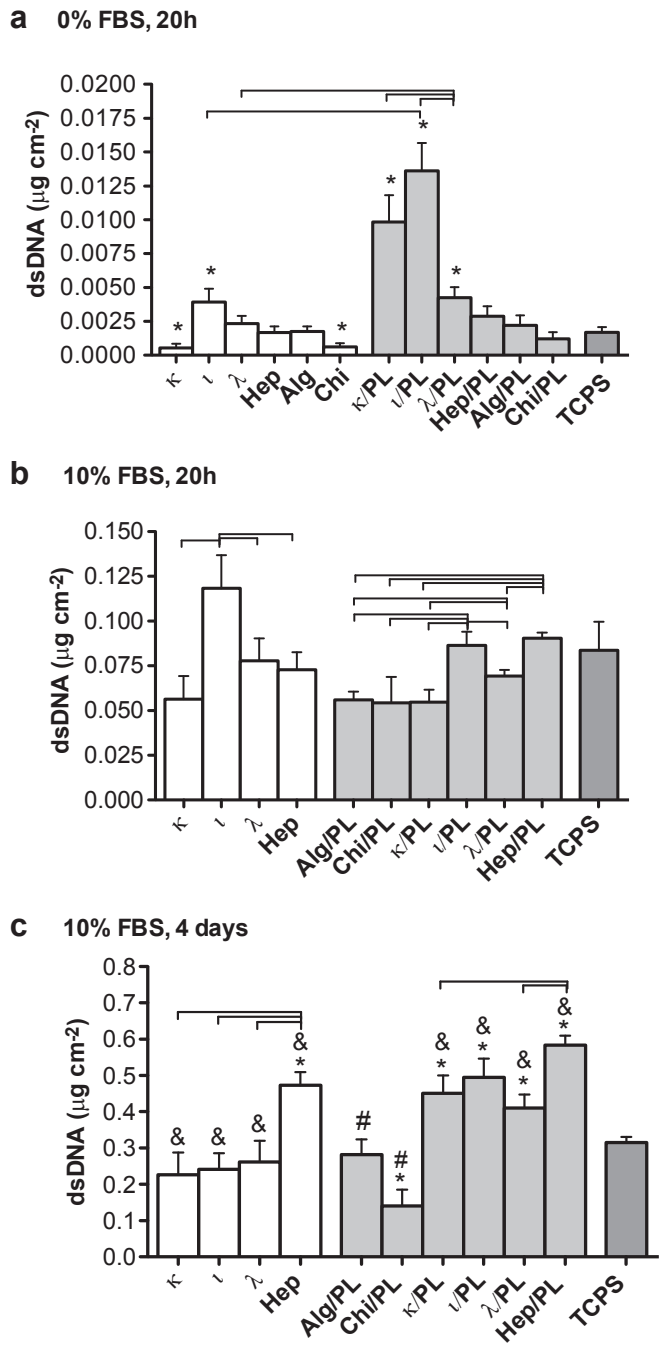

Fig. 5. hASCs adhesion and proliferation after 20 h and 4 days of culture. a) hASCs adhesion in serum free conditions after 20 h in culture. b) hASCs adhesion in presence of 10% FBS. c) dsDNA content after 4 days in culture. All the significances are identified: bars (the samples are different), * (different from TPCS), # (different to all other samples with PL), & (sample PE1/PL is different to PE1); ($p \leq 0.05$; $n = 10$; 2 donors). Data represented as mean ± SEM.

culture time although, at different extents depending on the coating. On κ, λ, ι/PL, λ/PL and the Hep/PL nanocoatings, ALP activity increase was much lower than TCPS ($p < 0.05$). The variations in ALP activity, upon 4 days in culture, were not correlated with cell content, proliferation, GFs and PL content, nor with the assessed morphological features – see Table S2. Nevertheless, there was a moderate positive correlation between the samples with and without PL, which also denotes the importance of the surface chemistry. One cannot exclude that the PE coatings may have adsorb similar proteins from media serum, although in lower concentration. The overall variations in ALP may be related with the presence of other proteins, or proteins ratios not contemplated in the analysis. ALP activity has been shown to vary with the ratio of the GFs used as medium supplement. For instance, FGFb has been reported to decrease ALP activity when used as media supplement, as opposed to VEGF [56]. When FGFb was combined with VEGF, the ALP activity reached values within the range of VEGF and FGFb alone but, lower than the increased value when cultured only with VEGF [56]. Herein, as mentioned above, there was no correlation between FGF/VEGF ratio and the ALP variations. This suggests that other important factors, not contemplated in the analysis, may have been decisive for hASCs behavior.

Different combinations of PE and PL could be used to tune the ALP activity and proliferation and translate different osteogenic potentials in longer-term cultures.

3.4. hASCs phenotype

Cultured population of hASCs are strongly characterized by being positive to CD105, CD90 and CD73 regardless of their passage or time in culture and weak or negative for CD34 and CD31 [57,58]. Within lower passages the multipotency and the proliferation capability is not altered. However, the cell phenotype changes: both CD34 and CD31 expression declines, being accompanied by an increase of CD90 and CD105 [57,58]. Suga et al. [59] reported that the expression of CD34 in hASCs can be reversed. hASCs lost CD34 expression upon culturing with DMEM but regained expression after being cultured with endothelial basal medium [59]. The same authors also suggested that the loss of CD34 may be related with the physiological process of commitment and/or differentiation from immature status into specific lineages such as adipose, bone and smooth muscle [59]. The hASCs phenotype was characterized before seeding (P5–P6) and after 4 days in culture, on some of the multilayers that showed improved cell proliferation: ι/PL and κ/PL using TPCS and ι as controls. Results in Table 1 are shown as the variation on the percentage of each CD with the culture on each respective surface, in relation to the original phenotype before seeding.

TCPS showed the common trend of decreasing CD34, CD31 and CD45 positive cells while increasing CD105 and CD73 positive cells. On the other hand, SO_3H and PL interfered with the percentage of CD31 and CD34 positive cell. A plausible reason for such variation would be the binding of CD31/CD34 positive cells (positive cells for VEGF receptor) mediated by VEGF or other specific GFs that had been incorporated.

The results suggest less sulfated nanocoatings as more beneficial for cell proliferation applications. Whereas higher sulfated coatings might be more suitable for differentiation purposes or, more specifically, for bone and vascular engineering, since they present higher FGF/PDGF and VEGF/PDGF ratios.

4. Conclusions

hASCs are anchorage-dependent cells and the interactions with the biomaterial surface dictate their behavior and fate. PL is a cost-effective source of several autologous bioactive proteins, e.g. GFs. Herein, we show the preparation of cell instructive multilayers by assembling PL with several PEs using LbL.

The PE nature and the SD, are important features that have influenced the adsorption of PL, VEGF, FGFb and PDGF. Intermediate sulfated polysaccharides were more prompt for high FGFb, VEGF and PDGF incorporation. The low sulfated polysaccharides could adsorb high PDGF and intermediate VEGF, while Hep showed only high VEGF adsorption. Consequently, by increasing the SD, the VEGF/PDGF and

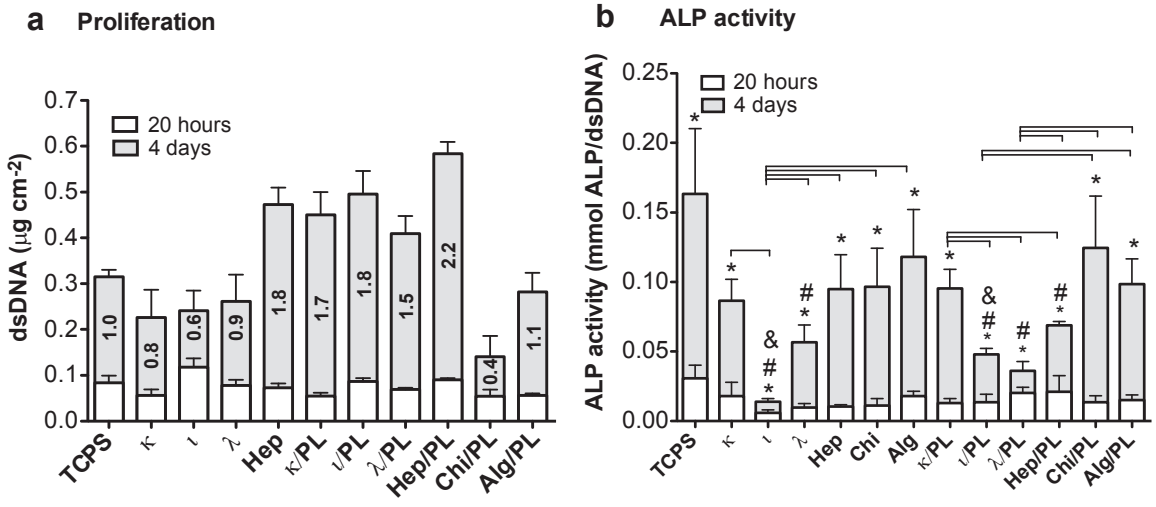

Fig. 6. hASCs proliferation ratios and ALP activity after 20 h and after 4 days of culture on the nanocoatings. a) Each set of superimposed bars show the dsDNA content at 20 h and 4 days with the proliferation ratios (relative to TCPS) indicated in the bars inset; b) Each set of superimposed bars corresponds to the ALP/cell after 20 h and 4 days in culture. All the statistical significances are identified: bars refer to the data of 4 days in culture, * (ALP varied from 20 h to 4 days), # (ALP at 4 days is different from ALP on TCPS 4 days), & (ALP on sample PE1/PL is different to PE1, after 4 days in culture); ($p \leq 0.05$; $n = 10$; 2 donors). Data presented as mean ± SEM.

Table 1
Flow cytometry assessment of the phenotype changes between P5-6 to P6-7 when cultured on the nanocoatings or TCPS for 4 days. Table shows the CD (Cluster of Differentiation) variation comparing with the phenotype before seeding (mean ± SD; 2 donors).

	TCPS	ι	ι/PL	κ/PL
CD105	0.0 ± 0.1	−1.6 ± 0.5	−1.3 ± 0.9	−1.2 ± 0.0
CD73	0.2 ± 0.1	−0.3 ± 0.4	−0.4 ± 0.8	−1.0 ± 0.4
CD90	0.0 ± 0.1	0.2 ± 0.2	0.2 ± 0.2	−0.8 ± 0.2
CD45	−0.4 ± 0.2	0.2 ± 0.7	−0.6 ± 0.9	−2.2 ± 0.6
CD34	−0.3 ± 0.1	1.0 ± 2.4	0.5 ± 1.7	−1.3 ± 0.2
CD31	−0.2 ± 0.9	1.9 ± 2.4	1.4 ± 2.9	0.2 ± 0.4

FGF/PDGF ratios tended to increase. Overall, the biomimetic sulfated PL-multilayers were shown to be efficient in the promotion of morphological changes, serum-free cell adhesion and cell proliferation. The results highlight the importance of the initial surface chemistry regarding the incorporation of platelets derivatives into biomaterials. For instance, the more sulfated PL nanocoatings might be more adequate for vascular or differentiation purposes since they permit a lower FGFb and PDGF incorporation than the less sulfated ones. The specific interactions of the PL containing coatings with endothelial cells will be investigated in future work.

Acknowledgments

Portuguese Foundation for Science and Technology is gratefully acknowledged for fellowships of Sara M. Oliveira. (SFRH/BD/70107/2010).

The research leading to these results has received funding from the European Union's Seventh Framework Programme (FP7/2007–2013) under grant agreement no REGPOT-CT2012-316331-POLARIS and FP7-KBBE-2010-4-266033 – SPECIAL. This work was also supported by the European Research Council grant agreement ERC-2012-ADG 20120216-321266 for the project ComplexiTE. The authors acknowledge Rogério P. Pirraco for the Flow cytometry analysis.

Appendix A. Supplementary data

Supplementary data related to this article can be found at http://dx.doi.org/10.1016/j.biomaterials.2015.01.020.

References

[1] Guilak F, Cohen DM, Estes BT, Gimble JM, Liedtke W, Chen CS. Control of stem cell fate by physical interactions with the extracellular matrix. Cell Stem Cell 2009;5:17–26.
[2] Alves NM, Pashkuleva I, Reis RL, Mano JF. Controlling cell behavior through the design of polymer surfaces. Small 2010;6:2208–20.
[3] Custódio CA, Reis RL, Mano JF. Engineering biomolecular microenvironments for cell instructive biomaterials. Adv Health Mater 2014 [n/a–n/a].
[4] Buck CA, Horwitz AF. Cell surface receptors for extracellular matrix molecules. Annu Rev Cell Bio 1987;3:179–205.
[5] Lee K, Silva EA, Mooney DJ. Growth factor delivery-based tissue engineering: general approaches and a review of recent developments. J R Soc Interf 2011;8:153–70.
[6] Bishop JR, Schuksz M, Esko JD. Heparan sulphate proteoglycans fine-tune mammalian physiology. Nature 2007;446:1030–7.
[7] Henry TD, Annex BH, McKendall GR, Azrin MA, Lopez JJ, Giordano FJ, et al. The VIVA Trial Vascular endothelial growth factor in ischemia for vascular angiogenesis. Circulation 2003;107:1359–65.
[8] Eppler SM, Combs DL, Henry TD, Lopez JJ, Ellis SG, Yi JH, et al. A target-mediated model to describe the pharmacokinetics and hemodynamic effects of recombinant human vascular endothelial growth factor in humans. Clin Pharm Ther 2002;72:20–32.
[9] Pohl TL, Schwab EH, Cavalcanti-Adam EA. Covalent binding of BMP-2 on surfaces using a self-assembled monolayer approach. JoVE 2013:e50842-e.
[10] Thorey F, Menzel H, Lorenz C, Gross G, Hoffmann A, Windhagen H. Osseointegration by bone morphogenetic protein-2 and transforming growth factor beta2 coated titanium implants in femora of New Zealand white rabbits. Ind J Orthop 2011;45:57.
[11] Liu S, Liu T, Chen J, Maitz M, Chen C, Huang N. Influence of a layer-by-layer-assembled multilayer of anti-CD34 antibody, vascular endothelial growth factor, and heparin on the endothelialization and anticoagulation of titanium surface. J Biomed Mater Res Part A 2012;101:1144–57.
[12] Shah NJ, Hong J, Hyder MN, Hammond PT. Osteophilic multilayer coatings for accelerated bone tissue growth. Adv Mater 2012;24:1445–50.
[13] Crouzier T, Ren K, Nicolas C, Roy C, Picart C. Layer-By-layer films as a biomimetic reservoir for rhBMP-2 delivery: controlled differentiation of myoblasts to osteoblasts. Small 2009;5:598–608.
[14] Almodóvar J, Guillot R, Monge C, Vollaire J, Selimović Š, Coll J-L, et al. Spatial patterning of BMP-2 and BMP-7 on biopolymeric films and the guidance of muscle cell fate. Biomaterials 2014;35:3975–85.
[15] Wang H, Yin T, Ge S, Zhang Q, Dong Q, Lei D, et al. Biofunctionalization of titanium surface with multilayer films modified by heparin-VEGF-fibronectin complex to improve endothelial cell proliferation and blood compatibility. J Biomed Mater Res Part A 2013;101:413–20.
[16] De Cock LJ, De Koker S, De Vos F, Vervaet C, Remon J-P, De Geest BG. Layer-by-layer incorporation of growth factors in decellularized aortic heart valve leaflets. Biomacromolecules 2010;11:1002–8.
[17] Marx RE, Carlson ER, Eichstaedt RM, Schimmele SR, Strauss JE, Georgeff KR. Platelet-rich plasma: growth factor enhancement for bone grafts. Oral Surg Oral Med Oral Pathol Oral Radiol Endodontol 1998;85:638–46.
[18] Weibrich G, Kleis WK, Hafner G, Hitzler WE. Growth factor levels in platelet-rich plasma and correlations with donor age, sex, and platelet count. J Cranio-Maxillofacial Surg 2002;30:97–102.

[19] Andia I, Maffulli N. Platelet-rich plasma for managing pain and inflammation in osteoarthritis. Nat Rev Rheum 2013;9:721–30.
[20] Chen L, Yang X, Huang G, Song D, Ye X-S, Xu H, et al. Platelet-rich plasma promotes healing of osteoporotic fractures. Orthopedics 2013;36:e687–94.
[21] Kawasumi M, Kitoh H, Siwicka K, Ishiguro N. The effect of the platelet concentration in platelet-rich plasma gel on the regeneration of bone. J Bone Jt Surg, Br Volume 2008;90:966–72.
[22] Man Y, Wang P, Guo Y, Xiang L, Yang Y, Qu Y, et al. Angiogenic and osteogenic potential of platelet-rich plasma and adipose-derived stem cell laden alginate microspheres. Biomaterials 2012;33:8802–11.
[23] Santo VE, Duarte ARC, Popa EG, Gomes ME, Mano JF, Reis RL. Enhancement of osteogenic differentiation of human adipose derived stem cells by the controlled release of platelet lysates from hybrid scaffolds produced by supercritical fluid foaming. J Control Release 2012;162:19–27.
[24] Leotot J, Coquelin L, Bodivit G, Bierling P, Hernigou P, Rouard H, et al. Platelet lysate coating on scaffolds directly and indirectly enhances cell migration, improving bone and blood vessel formation. Acta biomater 2013;9:6630–40.
[25] Custódio C, Santo V, Oliveira M, Gomes M, Reis R, Mano J. Functionalized microparticles producing scaffolds in combination with cells. Adv Func Mater 2013;24(10):1391–400.
[26] Hudalla GA, Murphy WL. Biomaterials that regulate growth factor activity via bioinspired interactions. Adv Func Mater 2011;21:1754–68.
[27] Boudou T, Crouzier T, Ren K, Blin G, Picart C. Multiple functionalities of polyelectrolyte multilayer films: new biomedical applications. Adv Mater 2010;22:441–67.
[28] Costa RR, Mano JF. Polyelectrolyte multilayered assemblies in biomedical technologies. Chem Soc Rev 2014;43:3453–79.
[29] Shah NJ, Macdonald ML, Beben YM, Padera RF, Samuel RE, Hammond PT. Tunable dual growth factor delivery from polyelectrolyte multilayer films. Biomaterials 2011;32:6183–93.
[30] Crouzier T, Sailhan F, Becquart P, Guillot R, Logeart-Avramoglou D, Picart C. The performance of BMP-2 loaded TCP/HAP porous ceramics with a polyelectrolyte multilayer film coating. Biomaterials 2011;32:7543–54.
[31] Sakiyama-Elbert SE, Hubbell JA. Controlled release of nerve growth factor from a heparin-containing fibrin-based cell ingrowth matrix. J Control Release 2000;69:149–58.
[32] Ye XF, Wang HZ, Zhou JX, Li HQ, Liu J, Wang Z, et al. The effect of heparin-VEGF multilayer on the biocompatibility of decellularized aortic valve with platelet and endothelial progenitor cells. Plos One 2013;8.
[33] Cai S, Liu Y, Zheng Shu X, Prestwich GD. Injectable glycosaminoglycan hydrogels for controlled release of human basic fibroblast growth factor. Biomaterials 2005;26:6054–67.
[34] Rada T, Reis RL, Gomes AE. Novel method for the isolation of adipose stem cells (ASCs). J Tissue Eng Reg Med 2009;3:158–9.
[35] Vlodavsky I, Miao H-Q, Medalion B, Danagher P, Ron D. Involvement of heparan sulfate and related molecules in sequestration and growth promoting activity of fibroblast growth factor. Cancer Metastasis Rev 1996;15:177–86.
[36] Volkin DB, Tsai P, Dabora JM, Gress JO, Burke CJ, Linhardt RJ, et al. Physical stabilization of acidic fibroblast growth factor by polyanions. Arch Biochem Biophys 1993;300:30–41.
[37] Folkman J, Shing Y. Control of angiogenesis by heparin and other sulfated polysaccharides. Heparin and related polysaccharides. Springer; 1992. p. 355–64.
[38] Borges J, Mano JF. Molecular interactions driving the layer-by-layer assembling of multilayers: a review. Chem Rev 2014;114(18):8883–942.
[39] Yao X, Peng R, Ding J. Effects of aspect ratios of stem cells on lineage commitments with and without induction media. Biomaterials 2013;34:930–9.
[40] Connelly JT, Gautrot JE, Trappmann B, Tan DW-M, Donati G, Huck WT, et al. Actin and serum response factor transduce physical cues from the microenvironment to regulate epidermal stem cell fate decisions. Nat Cell Biol 2010;12:711–8.
[41] Treiser MD, Yang EH, Gordonov S, Cohen DM, Androulakis IP, Kohn J, et al. Cytoskeleton-based forecasting of stem cell lineage fates. Proc Nat Acad Sci 2010;107:610–5.
[42] Kumar G, Tison CK, Chatterjee K, Pine PS, McDaniel JH, Salit ML, et al. The determination of stem cell fate by 3D scaffold structures through the control of cell shape. Biomaterials 2011;32:9188–96.
[43] Banfi A, Muraglia A, Dozin B, Mastrogiacomo M, Cancedda R, Quarto R. Proliferation kinetics and differentiation potential of ex vivo expanded human bone marrow stromal cells: implications for their use in cell therapy. Exp Hematol 2000;28:707–15.
[44] Cholewa D, Stiehl T, Schellenberg A, Bokermann G, Joussen S, Koch C, et al. Expansion of adipose mesenchymal stromal cells is affected by human platelet lysate and plating density. Cell Transplant 2011;20:1409–22.
[45] Griffiths S, Baraniak PR, Copland IB, Nerem RM, McDevitt TC. Human platelet lysate stimulates high-passage and senescent human multipotent mesenchymal stromal cell growth and rejuvenation in vitro. Cytotherapy 2013;15:1469–83.
[46] Chen G, Shi X, Sun C, Li M, Zhou Q, Zhang C, et al. VEGF-mediated proliferation of human adipose tissue-derived stem cells. PloS One 2013;8:e73673.
[47] Hebert TL, Wu X, Yu G, Goh BC, Halvorsen YDC, Wang Z, et al. Culture effects of epidermal growth factor (EGF) and basic fibroblast growth factor (bFGF) on cryopreserved human adipose-derived stromal/stem cell proliferation and adipogenesis. J Tissue Eng Reg Med 2009;3:553–61.
[48] Horn P, Bokermann G, Cholewa D, Bork S, Walenda T, Koch C, et al. Impact of individual platelet lysates on isolation and growth of human mesenchymal stromal cells. Cytotherapy 2010;12:888–98.
[49] Qiu P, Song W, Niu Z, Bai Y, Li W, Pan S, et al. Platelet-derived growth factor promotes the proliferation of human umbilical cord-derived mesenchymal stem cells. Cell Biochem Funct 2013;31:159–65.
[50] Heldin C-H, Wasteson Å, Westermark B. Platelet-derived growth factor. Mol Cell Endocrinol 1985;39:169–87.
[51] Kim M, Kim YH, Tae G. Human mesenchymal stem cell culture on heparin-based hydrogels and the modulation of interactions by gel elasticity and heparin amount. Acta Biomater 2013;9:7833–44.
[52] Furue MK, Na J, Jackson JP, Okamoto T, Jones M, Baker D, et al. Heparin promotes the growth of human embryonic stem cells in a defined serum-free medium. Proc Nat Acad Sci 2008;105:13409–14.
[53] Hirai H, Katoku-Kikyo N, Karian P, Firpo M, Kikyo N. Efficient iPS cell production with the MyoD transactivation domain in serum-free culture. PloS One 2012;7:e34149.
[54] Golub EE, Boesze-Battaglia K. The role of alkaline phosphatase in mineralization. Curr Opin Orthop 2007;18:444–8.
[55] Li Z, Liu C, Xie Z, Song P, Zhao RC, Guo L, et al. Epigenetic dysregulation in mesenchymal stem cell aging and spontaneous differentiation. PloS One 2011;6:e20526.
[56] Lee J-H, Um S, Jang J-H, Seo BM. Effects of VEGF and FGF-2 on proliferation and differentiation of human periodontal ligament stem cells. Cell Tissue Res 2012;348:475–84.
[57] Mitchell JB, McIntosh K, Zvonic S, Garrett S, Floyd ZE, Kloster A, et al. Immunophenotype of human adipose-derived cells: temporal changes in stromal-associated and stem cell-associated markers. Stem Cells 2006;24:376–85.
[58] Yoshimura K, Shigeura T, Matsumoto D, Sato T, Takaki Y, Aiba-Kojima E, et al. Characterization of freshly isolated and cultured cells derived from the fatty and fluid portions of liposuction aspirates. J Cell Physiol 2006;208:64–76.
[59] Suga H, Matsumoto D, Eto H, Inoue K, Aoi N, Kato H, et al. Functional implications of CD34 expression in human adipose-derived stem/progenitor cells. Stem Cells Dev 2009;18:1201–10.